ACS Photonics

Article

pubs.acs.org/journal/apchd5

Quality Factor of Luminescent Solar Concentrators and Practical Concentration Limits Attainable with Semiconductor Quantum Dots

Victor I. Klimov,*[,†] Thomas A. Baker,[†] Jaehoon Lim,[†] Kirill A. Velizhanin,[‡] and Hunter McDaniel[§]

[†]Center for Advanced Solar Photophysics, Chemistry Division, and [‡]Center for Advanced Solar Photophysics, Theoretical Division, Los Alamos National Laboratory, Los Alamos, New Mexico 87545, United States

[§]UbiQD, LLC, 134 East Gate Drive, Los Alamos, New Mexico 87544, United States

Supporting Information

ABSTRACT: Luminescent solar concentrators (LSCs) can be utilized as both large-area collectors of solar radiation supplementing traditional photovoltaic cells as well as semitransparent "solar windows" that provide a desired degree of shading and simultaneously serve as power-generation units. An important characteristic of an LSC is a concentration factor (C) that can be thought of as a coefficient of effective enlargement (or contraction) of the area of a solar cell when it is coupled to the LSC. Here we use analytical and numerical Monte Carlo modeling in addition to experimental studies of quantum-dot-based LSCs to analyze the factors that influence optical concentration in practical devices. Our theoretical model indicates that the maximum value of C achievable with a given fluorophore is directly linked to the LSC quality factor (Q_{LSC}) defined as the ratio of absorption coefficients at the wavelengths of incident and reemitted light. In fact, we demonstrate that the ultimate concentration limit (C_0) realized in large-area devices scales linearly with the LSC quality factor and in the case of perfect emitters and devices without back reflectors is approximately equal to Q_{LSC}. To test the predictions of this model, we conduct experimental studies of LSCs based on visible-light emitting II–VI core/shell quantum dots with two distinct LSC quality factors. We also investigate devices based on near-infrared emitting $CuInSe_xS_{2-x}$ quantum dots for which the large emission bandwidth allows us to assess the impact of varied Q_{LSC} on the concentration factor by simply varying the detection wavelength. In all cases, we find an excellent agreement between the model and the experimental observations, suggesting that the developed formalism can be utilized for express evaluation of prospective LSC performance based on the optical spectra of LSC fluorophores, which should facilitate future efforts on the development of high-performance devices based on quantum dots as well as other types of emitters.

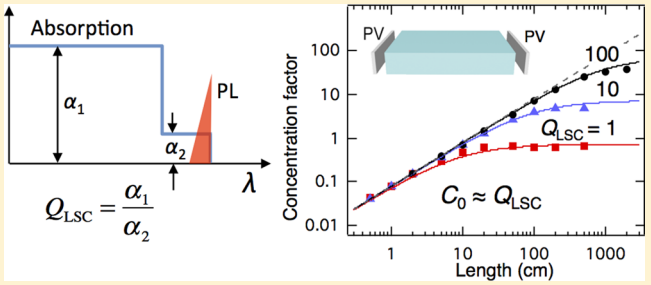

KEYWORDS: *luminescent solar concentrator, LSC, LSC quality factor, concentration factor, optical efficiency, quantum dot*

Luminescent solar concentrators (LSCs) are light management devices that consist of a large-area slab of a transparent materials serving as a low-loss waveguide impregnated (or coated) with highly luminescent fluorophores such as organic dyes, emitting ions, or quantum dots (Figure 1a).[1−6] As illustrated in Figure 1a,b, light impinging onto a large-area front side of the slab (incident photon flux Φ_1) is absorbed by the fluorophores and reemitted at a longer wavelength. Even without special reflecting coatings, a significant fraction of emitted radiation (~75% for a refractive index of 1.5) is trapped by total internal reflection (process 1 in Figure 1a) and wave-guided toward the edges of the slab where it can be collected (flux Φ_2) by photovoltaic (PV) cells (Figure 1a,b). Due to a potentially large difference between the area of the front surface of the slab exposed to solar light (A_1) and the area of its edges (A_2), this device serves as a solar concentrator, that is, it can increase the flux density incident onto the PV ($\phi_2 = \Phi_2/A_2$) compared to the original flux density ($\phi_1 = \Phi_1/A_1$); Figure 1b. In quantitative terms, the LSC concentration factor C is defined as $C = \phi_2/\phi_1$, which can be rewritten as $C = G\eta_{opt}$, where $G = A_1/A_2 = L/(2d)$ is a geometric gain factor (L and d are the LSC length and thickness, respectively; Figure 1b) and $\eta_{opt} = \Phi_2/\Phi_1$ is the LSC optical efficiency or the external quantum efficiency of the device. The C-factor can be thought of as an effective enlargement (or contraction) factor of an area of a PV device when it is coupled to an LSC. In the ideal case of $\eta_{opt} = 1$, C is equal to the geometric gain factor.

When C is greater than 1, the use of an LSC leads to increased photocurrent if compared to the situation where the PV is directly exposed to sunlight. An important advantage of LSCs as light-collecting devices is that they are active under both direct and diffuse illumination, while traditional mirror- or lens-based concentrators operate only under direct solar illumination and thus require high-precision tracking. On the other hand, while traditional concentration allows for increased power conversion efficiency due to the increased photovoltage, the LSC does not provide this advantage, as in the ideal

Received: April 28, 2016
Published: May 9, 2016

DOI: 10.1021/acsphotonics.6b00307
ACS Photonics 2016, 3, 1138−1148

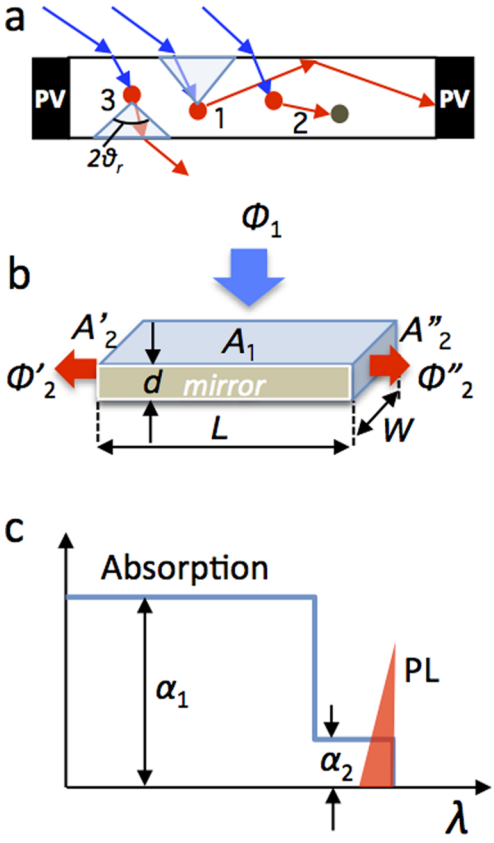

Figure 1. Schematic depiction of LSC operation. (a) Incident light (blue arrows) with wavelength λ_1 is absorbed by fluorophores (circles) embedded into a transparent waveguide and reemitted at a longer wavelength λ_2 (red arrows). Reemitted photons can be either trapped by total internal reflection and waveguided to PVs at device edges (pathway 1) or lost due to nonradiative recombination following reabsorption (pathway 2) or "leakage" through the escape cone with the size defined by the angle of total internal reflection θ_r (pathway 3). (b) Fraction of incident flux (Φ_1) impinging onto a front surface (area A_1) is absorbed by LSC fluorophores, reemitted, and guided toward PV devices on the left (output flux Φ'_2; area A'_2) and the right (output flux Φ''_2; area A''_2) edges of the device. The geometric gain factor (G) is defined by the ratio of A_1 and $A_2 = A'_2 + A''_2$. (c) Stepwise absorption profile (blue line) of an "ideal" LSC fluorophore characterized by a small absorption coefficient (α_2) at longer wavelengths within the emission band (red shading) and a large absorption coefficient ($\alpha_1 \gg \alpha_2$) at shorter wavelengths.

"radiative limit" the increase in the flux density is exactly compensated by increasing losses due to intrinsic radiative recombination, and therefore, the open-circuit voltage remains unchanged.[7,8] Thus, the use of LSC light collectors, while potentially leading to a boost in a photocurrent, does not allow one to exceed the traditional Shockley-Queisser limit for nonconcentrating PVs.[9]

A potentially advantageous feature of LSCs is also their ability to reshape the spectrum of solar radiation for improving its match to the spectral characteristics of a specific PV. For example, some of the Si solar cells exhibit a decline in the power conversion efficiency on the blue side of the solar spectrum due to the reduction in the absorption length and the concomitant enhancement of surface recombination. The LSC can help mitigate this problem by downshifting the radiation wavelength, ideally to the position, which matches the peak in the spectral response of the solar cell.

In addition to serving as high-efficiency light collectors and spectral reshapers of incident radiation for traditional PVs, LSCs can also enable novel energy conversion devices such as solar (or photovoltaic) windows that provide a desired degree of shading and/or coloring while also serving as power-generation units. Practical implementation of the "solar-window" ideas can become an important element of ongoing efforts on the realization of the concept of net-zero-energy-consumption buildings.[5,6,10−12]

After the introduction of the LSC concept in 1976 by Weber and Lambe,[1] this topic has been actively explored both experimentally and theoretically. Initial experimental efforts have focused primarily on dye-based LSCs.[3,5,13,14] However, more recently a significant attention has been directed toward LSCs based on colloidal quantum dots (QDs).[11,15−25] The main motivation for exploring QDs in the context of LSCs is derived from the flexibility afforded by these structures in controlling their optical absorption and emission spectra. Specifically, using appropriately designed QDs, one can considerably reduce losses due to reabsorption of the waveguided radiation, which is a significant problem with traditional dyes that are characterized by a significant overlap between the photoluminescence (PL) and absorption bands. QDs are also attractive for LSC applications as there are a number of systems (e.g., based on II−III−VI_2 and IV−VI semiconductors) that allow for high emission efficiencies (>50−90% quantum yields) in the near-infrared region of the optical spectrum,[26−31] which is well suited for coupling to traditional Si solar cells. This is in stark contrast to organic dyes that are very poor infrared emitters due to significant losses to nonradiative recombination in the case of small HOMO−LUMO gaps.

The reduced overlap between absorption and emission spectra has been often associated with a large Stokes shift and so the efforts on reducing losses to reabsorption have been termed "Stokes-shift engineering." Several strategies have been proposed and successfully employed for increasing an apparent Stokes shift in QDs including shape control (demonstrated with, e.g., nanorods),[19] incorporation of intragap emissive impurities,[17] and use of core−shell nanocrystals.[16,21,22] The latter strategy, for example, was applied in ref 21, where high-efficiency LSCs were realized using thick-shell (so-called "giant") CdSe/CdS QDs. In these structures, the absorption and emission functions are separated between a wider-gap shell and a narrower-gap core which results in the large apparent Stokes shift of >400 meV. More recently, QDs of ternary I−III−VI_2 semiconductors ($CuInE_2$, where E = S or Se or their mixture) were explored in the context of LSCs as a heavy-metal-free alternative to Cd-based nanocrystals.[11,23,32] In these materials, reabsorption losses are reduced due to the involvement of an intragap hole state (associated likely with a native Cu-related defect[33]) in the emission process, which leads to a large spectral displacement of the PL band with respect to the onset of strong interband absorption.

While the apparent Stokes shift does provide qualitative guidance in selecting an appropriate LSC fluorophore, its value does not allow one to assess the prospective LSC performance in quantitative terms. To find a more rigorous characteristic for evaluating LSC fluorophores, we have turned our attention to the spectral shape of optical absorption. It is apparent and widely recognized that for the best performance, the LSC fluorophores should exhibit a step-like absorption profile with a large absorption coefficient at the wavelength (λ_1) of collected

DOI: 10.1021/acsphotonics.6b00307
ACS Photonics 2016, 3, 1138−1148

radiation, $\alpha_1 = \alpha(\lambda_1)$, and a much smaller absorption coefficient at the wavelength (λ_2) of the emitted light, $\alpha_2 = \alpha(\lambda_2)$ (Figure 1c). This suggests that the ratio of α_1 and α_2 might serve as a figure of merit or a *quality factor* of an LSC: $Q_{LSC} = \alpha_1/\alpha_2$. Here we show that this quantity can indeed be used to directly evaluate the prospective LSC performance of a fluorophore. Using a Monte Carlo (MC) ray-tracing simulation supplemented by an analytical model, we demonstrate that Q_{LSC} defines the ultimate concentration limit achievable with a given fluorophore. Specifically, the ultimate optical concentration factor (C_0), which is realized in the large-size limit, is directly proportional to Q_{LSC}, that is, $C_0 = FQ_{LSC}$, where $F \approx 1$ in the case of ideal LSC emitters with the PL quantum yield (η_{PL}) of unity and semitransparent devices without back reflectors. Using our formalism, based on a Q_{LSC} factor, we can predict an optimal slab absorptivity, which produces the maximum possible optical concentration for given LSC dimensions. This capability is useful in the case of both semitransparent LSC windows and high-concentration devices aimed at replacing traditional mirror/lens-based systems. We verify the predictions of the model by conducting measurements on LSCs containing visible-light emitting II−VI core/shell QDs with two distinct LSC quality factors. We also study devices that are based on near-infrared emitting $CuInSe_xS_{2-x}$ QDs. A large emission bandwidth of these QDs allows us to evaluate the affect of varied Q_{LSC} on the concentration factor by varying the PL detection wavelength. Both studied QD systems have been recently utilized in practical demonstrations of high-performance LSCs.[11,21−23,32]

PRACTICAL CONCENTRATION LIMITS OF PLANAR LSCs

Since the introduction of the concept of LSCs,[1] these structures have been the subject of numerous theoretical studies using thermodynamic and optical approaches.[3,4,7,8,20,34−39] It was shown that, on the basis of the second law of thermodynamics, the ultimate concentration limit, or thermodynamic limit (C_{th}), is directly related to the energy loss during the down-conversion process. This energy, sometimes referred to as a Stokes shift, is defined as the difference in photon energies for incident and reemitted radiation, $\Delta_S = ch(\lambda_1^{-1} - \lambda_2^{-1})$; here c is the speed of light and h is the Planck constant. Based on thermodynamic considerations, $C_{th} = (\lambda_1/\lambda_2)^3 \exp(\Delta_S/k_BT)$, where k_B is the Boltzmann constant and T is the ambient temperature.[34,35] According to this expression, for a red-emitting fluorophore with a moderate Stokes shift of 200 meV, C_{th} is ∼3000, which is far beyond of any practically demonstrated values that are still in the range of a few tens.[18] The realization of the thermodynamic concentration limit would require ideal fluorophores with a 100% PL quantum yield and an ideal LSC cavity, which is transparent for incident light while perfectly trapping the reradiated light. The latter can be accomplished using a wavelength-selective mirror or a so-called "selective reflector" installed on top of the LSC face exposed to solar light. These reflectors should be designed such as to provide high (ideally 100%) transmittance over the range of wavelengths absorbed by the LSC and at the same time serve as perfect reflectors for light emitted by LSC fluorophores.[40]

Current LSC systems are still far from these ideal requirements. Therefore, the practical concentration limits are typically analyzed using optical modeling that attempts to capture various sources of losses associated with nonideal PL quantum yields and imperfections in the LSC waveguides. A common approach to this problem is MC ray-tracing simulations.[12,20,41,42] While being accurate and versatile, they can, however, be computationally intense and time-consuming, which complicates their use in the case of, for example, large-scale structures.

Here we attempt to develop a simple analytical approach for an express evaluation of prospective performance of LSCs, which could supplement MC simulations and in some cases even replace them. In our model, we consider a planar device with dimensions L (length), W (width), and d (height), with 100% reflecting mirrors on the sidewalls (Figure 1b). We treat the top and bottom LSC surfaces as standard air/glass interfaces and assume perfect light outcoupling (100% transmission) at the left and right device sides terminated with PVs. In this configuration, the output flux (Φ_2) is a sum of fluxes propagating in the left (Φ'_2) and the right (Φ''_2) directions ($\Phi_2 = \Phi'_2 + \Phi''_2$), while the output area is sum of the areas of the device left and right edges ($A_2 = A'_2 + A''_2$); Figure 1b. The geometric gain factor of this device is $G = L/(2d)$.

The LSC optical efficiency can be expressed as $\eta_{opt} = \eta_{abs}\eta_{col}$, where η_{abs} is the device absorptance (fraction of incident photons that are absorbed by the LSC fluorophores) and η_{col} is the collection efficiency (fraction of the absorbed photons that ultimately reach the output faces); η_{col} can be thought of as an internal quantum efficiency of an LSC, which defines the device efficiency per absorbed photon. The absorptance can be expressed via the reflection coefficient of the air/glass interface (R), and the absorption coefficient at the wavelength of incident light (α_1) as $\eta_{abs} = (1 - R)(1 - e^{-\alpha_1 d})$. The collection efficiency can be presented as $\eta_{col} = \eta_{PL}\eta_{trap}\eta_{wg}$, where η_{trap} is the efficiency of light trapping into waveguide modes and η_{wg} is a waveguiding efficiency defined as a fraction of the first-generation, waveguide-trapped PL photons that eventually reach the PV-terminated LSC edges. In the case of spatially isotropic emitters, $\eta_{trap} = \cos\theta_r$, where $\theta_r = \arcsin(1/n)$ is the angle of total internal reflection (n is the refractive index of the slab). Angle θ_r defines the size of a so-called escape cone (Figure 1a); for the glass/air interface $\theta_r = 41.8°$ and $\eta_{trap} = 0.75$.

In our model, we assume that the waveguding losses are solely due to reabsorption events that are followed by either nonradiative recombination (process 2 in Figure 1a) or emission into the escape cone (process 3 in Figure 1a). This approach does not account for extrinsic losses due to scattering at optical imperfection within the LSC slab. It also disregards a partial recovery of escape-cone losses due to the effect of reabsorption within the escape cone followed by emission into the waveguided modes. The first of these processes can be accounted for by introducing a "scattering correction" to α_2. As indicated by our numerical MC modeling (see below), the second process can be taken into account by introducing a constant factor of ∼1.05, which corrects for slight underestimation of the overall efficiency resulting from neglecting effects of reabsorption/re-emission within the escape cone.

The losses due to reabsorption in the absence of reemission were analyzed by Weber and Lambe in their original proposal of the LSC concept.[1] Their calculations can be approximated by a function $\eta_{wg}^{(1)} = 1/(1 + \beta\alpha_2 L)$ with $\beta = 1.4$, which provides a better than +12%/−15% accuracy in describing the exact solution for $\alpha_2 L$ up to 20 (see Figure S1 of Supporting Information, SI). Here we use this functional form of $\eta_{wg}^{(1)}$ to obtain an approximate analytical expression for the LSC

DOI: 10.1021/acsphotonics.6b00307
ACS Photonics 2016, 3, 1138−1148

efficiency, which accounts for repeating reabsorption-reemission events.

We start our analysis with the first-generation of PL photons that are produced following the absorption of original incident light. The fraction of these photons, which is eventually collected at the LSC edges, is directly linked to $\eta_{wg}^{(1)}$ by $\eta_{col}^{(1)} = \eta_{wg}^{(1)}\eta_{PL}\eta_{trap}$. The processes of reemission following absorption of waveguided radiation will increase the overall collection efficiency and can be accounted for by summing the contributions from the second, third, etc., re-emission events. To account for the second-generation of reemitted photons (collection efficiency $\eta_{col}^{(2)}$), we apply the first-generation collection efficiency $\eta_{col}^{(1)}$ to the fraction of the photons $(1 - \eta_{wg}^{(1)})$ removed from the propagating modes by the first reabsorption event. This leads to $\eta_{col}^{(2)} = \eta_{PL}\eta_{trap}(1 - \eta_{wg}^{(1)})\eta_{col}^{(1)}$.[4] Similarly, $\eta_{col}^{(3)} = [\eta_{PL}\eta_{trap}(1 - \eta_{wg}^{(1)})]^2\eta_{col}^{(1)}$, $\eta_{col}^{(4)} = [\eta_{PL}\eta_{trap}(1 - \eta_{wg}^{(1)})]^3\eta_{col}^{(1)}$, and so on. Thus, each $\eta_{col}^{(i)}$ term represents a member of a geometric progression expressed as $\eta_{col}^{(i)} = [\eta_{PL}\eta_{trap}(1 - \eta_{wg}^{(1)})]^{i-1}\eta_{col}^{(1)}$. The total collection efficiency can be found as a sum of contributions due to all photon generations, $\eta_{col} = \sum_{i=1}^{\infty}\eta_{col}^{(i)}$, which yields $\eta_{col} = \eta_{col}^{(1)}[1 - \eta_{PL}\eta_{trap}(1 - \eta_{wg}^{(1)})]^{-1}$. Replacing $\eta_{wg}^{(1)}$ with $(1 + \beta\alpha_2 L)^{-1}$ as discussed earlier, we obtain $\eta_{col} = \eta_{PL}\eta_{trap}[1 + \beta\alpha_2 L(1 - \eta_{PL}\eta_{trap})]^{-1}$. This leads to the following expressions for the optical efficiency and the concentration factor of a planar LSC:

$$\eta_{opt} = \frac{(1 - R)(1 - e^{-\alpha_1 d})\eta_{PL}\eta_{trap}}{1 + \beta\alpha_2 L(1 - \eta_{PL}\eta_{trap})} \quad (1)$$

$$C = \frac{(1 - R)(1 - e^{-\alpha_1 d})\eta_{PL}\eta_{trap}}{1 + \beta\alpha_2 L(1 - \eta_{PL}\eta_{trap})}\left(\frac{L}{2d}\right) \quad (2)$$

According to eq 2, at small L when $\alpha_2 L \ll 1$, the concentration factor is proportional to the device length, that is, scales linearly with the geometric gain factor. However, when $\alpha_2 L$ approaches unity and then exceeds it, the C-factor begins to saturate and asymptotically approaches the value given by

$$C_{sat} = \frac{(1 - R)}{2\beta(\eta_{PL}^{-1}\eta_{trap}^{-1} - 1)}\frac{(1 - e^{-\alpha_1 d})}{\alpha_2 d} \quad (3)$$

The maximum of C_{sat} is realized when $\alpha_1 d$ approaches 0, which defines an ultimate concentration limit (C_0) attainable with a given fluorophore for the device configuration shown in Figure 1b:

$$C_0 = \frac{(1 - R)}{2\beta(\eta_{PL}^{-1}\eta_{trap}^{-1} - 1)}\frac{\alpha_1}{\alpha_2} = FQ_{LSC} \quad (4)$$

where $F = (1 - R)[2\beta(\eta_{PL}^{-1}\eta_{trap}^{-1} - 1)]^{-1}$ is a numerical prefactor determined by the PL quantum yield and the refractive index of the LSC slab; the latter defines R and η_{trap}. In the case of ideal emitters ($\eta_{PL} = 1$) and the glass/air interface ($\eta_{trap} = 0.75$ and $R = 0.04$ for the normal incidence), $F = 1.45/\beta$ or $F \approx 1$, if $\beta = 1.4$, as determined from the fit to the Weber and Lambe model (Figure S1 of SI). This indicates that the maximum concentration factor achievable with a given fluorophore is directly proportional to Q_{LSC}, and furthermore, in the case of the ideal quantum yield, it is approximately equal to the LSC quality factor: $C_0 \approx Q_{LSC}$.

If an LSC application does not require a semitransparent device, a simple approach to increase the concentration factor is by installing a fully reflecting mirror at the back of the waveguide. This increases the device absorptance for incident radiation by doubling the light propagation path but at the same time preserves the geometric gain factor and the collection efficiency. The net result of these changes is the increased concentration factor. In the case of a device with $\alpha_1 d \ll 1$, the back reflector increases the absorptance by a factor of 2, which leads to the following expression for the ultimate concentration factor for this device architecture with a fully reflecting back side: $C_{0,ref} = 2FQ_{LSC}$. For the situation of the air/glass interface at the front LSC surface, $C_{0,ref} \approx 2.1Q_{LSC}$. Interestingly, when $Q_{LSC} = 1$, which corresponds to $\alpha_1 = \alpha_2$, the above expression yields C_0 of 2.1. This situation is somewhat analogous to a slab comprising neutral scattering centers that randomize the direction of incident radiation without changing its wavelength. Such a system can indeed be employed in LSCs;[43,44] however, due to conservation of etendue its concentration factor is limited by n^2, that is, ~ 2.25 in the case of a glass or a polymer waveguide. This value is remarkably close to the one predicated by our model ($C_{max} = 2.1$) for the case of $Q_{LSC} = 1$.

COMPARISON TO MONTE CARLO RAY-TRACING SIMULATIONS

To validate the above derivations, we conduct MC ray-tracing simulations (see SI, section 1) of devices depicted in Figure 1b assuming a fixed thickness and width ($d = W = 1$) cm and a varied length (L). We further set the optical density of the device at the wavelength of incident light (λ_1) to 0.1, which corresponds to $\alpha_1 = 0.23$ cm^{-1}. In Figure 2, we show the results of MC simulations (symbols) for the optical efficiency (panel "a") and the concentration factor (panel "b") as a function of L for three values of Q_{LCS} (1, 10, and 100) and the ideal PL quantum yield $\eta_{PL} = 1$. In the same figure, we also plot the results of the analytical model (lines) given by eqs 1 (η_{opt}) and 2 (C). To match the model to MC simulations at short distances, we introduce a constant multiplier b, which in all cases is equal to 1.05 (see Figure S2 of SI). As was discussed earlier, this accounts for a small (~5% in this case) underestimation of the optical efficiency by the analytical model, which occurs as a result of the disregard of PL photons produced by reabsorption events within the escape cone that are followed by reemission into the waveguided modes.

To describe the variation of η_{opt} with L, we have considered several values of β. With $\beta = 1.4$ (as derived from a fit to the Weber and Lambe model; Figure S1 of SI), analytical theory (dashed lines in Figure 2a) provides a good description of the results of the MC modeling for shorter distances (up to ~100 cm), but deviates at larger L. On the other hand, the use, for example, of $\beta = 1.8$ (dashed-and-dotted lines in Figure 2a) improves the agreement between the two models at large values of L (up to ~1000 cm), however, leads to some underestimation of η_{opt} at shorter L, which is especially pronounced for lower LSC quality factors (Q_{LSC} of 1−10). In order to better capture the behavior of η_{opt} across the entire range of distances used in our calculations, we have also considered the situation of a distance-dependent parameter β. For example, using expression $\beta = 1.4 + 0.5(L/150)^{1/2}$ (inset of Figure 2a), we have been able to obtain a nearly perfect match to the MC modeling across the range of distances $L = 0$−2000 cm (solid lines in Figure 2a). We would like to caution, however, that this expression is of limited applicability, as at very large L, it leads to the unphysical behavior of the concentration factor, which

DOI: 10.1021/acsphotonics.6b00307
ACS Photonics 2016, 3, 1138−1148

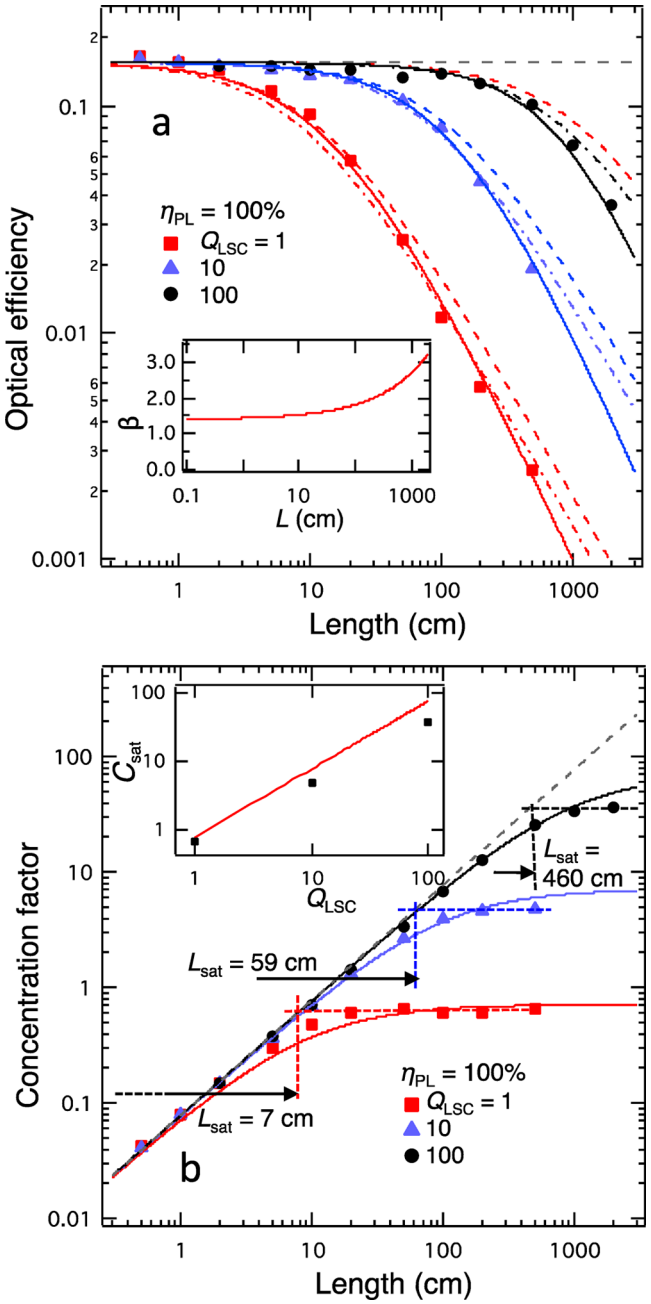

Figure 2. An optical efficiency (a) and a concentration factor (b) of an LSC as a function of device length (L) calculated using the analytical model (eqs 1 and 2; lines) and Monte Carlo (MC) simulations (symbols). The device thickness is 1 cm and the absorption coefficient at the wavelength of incident light is 0.23 cm^{-1}; these parameters correspond to about 80% transmission coefficient. The PL quantum yield of LSC fluorophores (η_{PL}) is assumed to be 100%. The calculations have been conducted for three different LSC quality factor (Q_{LSC}): 1 (red), 10 (blue), or 100 (black). The lines of three different styles in panel "a" correspond to different values of the β-coefficient: 1.4 (dashed), 1.8 (dashed-and-dotted), and L-dependent (varied according to the dependence in the inset of panel "a"). Inset of panel "b" shows a saturated concentration factor (C_{sat}) as a function of Q_{LSC} calculated using the analytical model (line; eq 3) and MC simulations (symbols).

instead of saturation shows a gradual decline with L. Therefore, in the analysis of concentration saturation of large devices (Figure 1b), we use a constant value of β equal to 1.8, given that it provides a closer match to the MC model compared to β = 1.4 at long distances. On the other hand, later in the paper, in the case of small-size LSCs (L < 10 cm), we will revert to β = 1.4.

The L-dependence of the concentration (Figure 2b) is a direct reflection of the L-dependence of the optical efficiency (Figure 2a). At short distance when η_{opt} is nearly constant, the C-factor shows an almost linear growth with L, that is, it scales directly with geometric gain $G = L/(2d)$. At longer L, when η_{opt} experiences a gradual drop, the concentration factor starts to saturate, approaching a constant value (C_{sat}). In agreement with the predictions of the analytical model (eq 3), C_{sat} obtained from the MC simulations scales almost linearly with the LSC quality factor (inset of Figure 2b). The LSC length at which the C-factor approaches its saturated value (L_{sat}) also scales directly with Q_{LSC}. We define this quantity from the intersection of the L-dependent "ideal" C-factor ($C \propto L$; gray dashed line in Figure 2b), with horizontal lines that correspond to C_{sat}. Based on the results of the MC calculations, L_{sat} increases from about 7 to 59 cm, and then 460 cm, for Q_{LSC} = 1, 10, and 100. The observed L_{sat} scaling (1:8.3:65) closely tracks changes in Q_{LSC}. The fact that the MC values of L_{sat} underestimate those from the analytical model is likely a result of insufficient accuracy of the MC modeling at large L. The increase in the length of the calculated trajectories leads to a rapid increase in the computation time, which makes it prohibitively more difficult to accumulate the sufficient amount of statistics required for an asymptotically exact solution.

We also find a close agreement between the analytical and the MC models in the case of nonunity PL quantum yields. This agreement is illustrated in Figure 3, where we show results of computations for Q_{LSC} = 10 and η_{PL} = 50, 70, 90, and 100%. Using b = 1.05 and β = 1.8, we obtain a close correspondence between the analytical model and MC simulations for all values of η_{PL} and across all distances up to 500 cm. As expected based on eq 3, the saturated concentration factor strongly depends on the PL quantum yield. In fact, for considered values $\eta_{PL} \geq$ 50%, C_{sat} scales almost as a square of η_{PL} (black line in the inset of Figure 3b). This behavior is consistent with one predicted by eq 3 (red line in the inset of Figure 3b). Specifically, according to this expression, the scaling of C_{sat} with η_{PL} is nearly linear at low PL quantum efficiencies, but it becomes superlinear at $\eta_{PL} \geq$ 40%. This highlights the importance of high PL quantum yields for obtaining high concentration factors in practical LSC devices. For example, by doubling η_{PL} from 40 to 80%, one can nearly quadruple both the LSC efficiency and the concentration factor.

To gain more insight into the effects of the PL quantum yield and the Q_{LSC} factor on the LSC performance, we replot the data from Figure 3a,b in the form of collection efficiency versus L (Figure 3c). We further define the maximum practical LSC length (L_0) as the distance at which η_{col} drops to 50%, that is, the LSC delivers to PVs 50% of the originally absorbed photons. Based on this definition, L_0 is 52 cm for η_{PL} = 100% and Q_{LSC} = 10. However, it reduces by nearly a half (to 29 cm) when the PL quantum yield is decreased by just 10% (to 90%). A further drop by nearly a factor of 6 (to $L_0 \approx$ 5 cm) occurs when η_{PL} is reduced to 70%. Finally, when η_{PL} is 50%, the condition η_{col} = 50% cannot be satisfied even at L = 0.

Interestingly, the drop in the PL quantum yield can be mitigated by increasing the LSC quality factor. For example, in the case of η_{PL} = 90%, by increasing Q_{LSC} to 18, it is possible to achieve the same value of L_0 as in the case of the ideal PL

DOI: 10.1021/acsphotonics.6b00307
ACS Photonics 2016, 3, 1138−1148

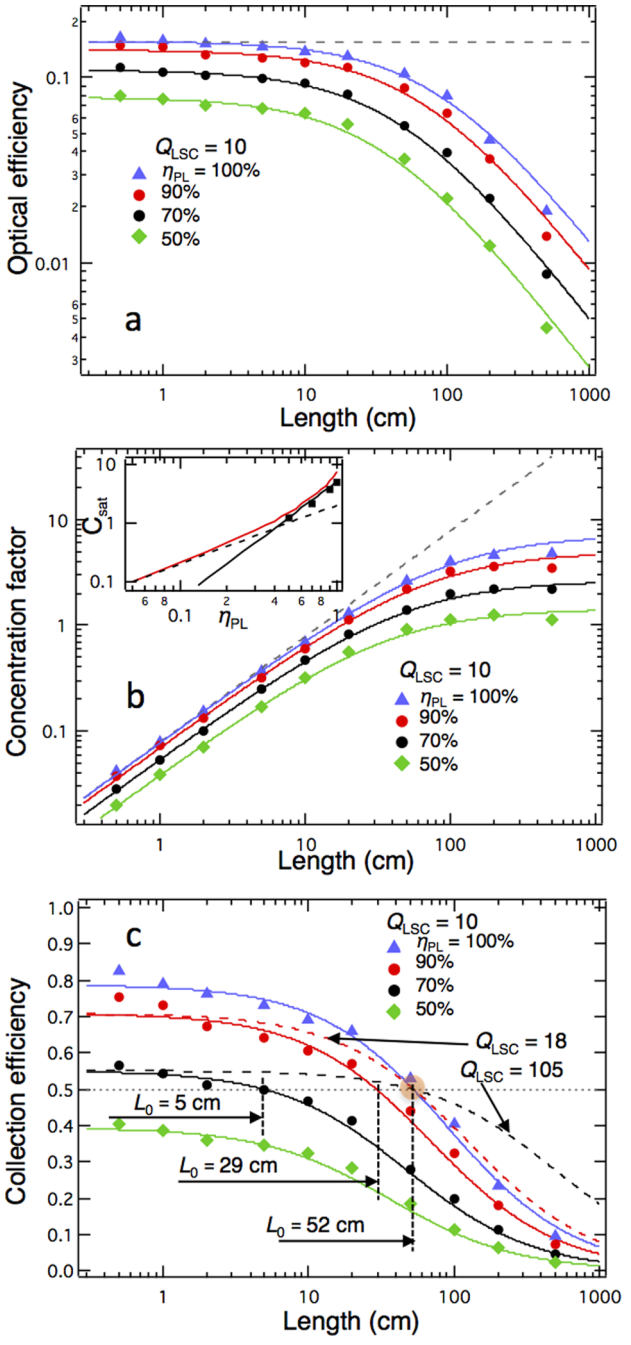

Figure 3. Optical efficiency (a), a concentration factor (b), and a collection efficiency (c) of an LSC as a function of L calculated using the analytical model (solid lines) and MC simulations (symbols) for Q_{LSC} = 10 and four quantum yields of the LSC fluorophores: 50% (green), 70% (black), 90% (red), and 100% (blue); same device dimensions and transmission coefficient as in Figure 2. The inset of panel "b" shows the dependence of the saturated concentration factor (C_{sat}) on η_{PL} based on the analytical model (red solid line) and MC simulations (symbols). The dependence of C_{sat} on η_{PL} changes from nearly linear at low values of η_{PL} (black dashed line) to nearly quadratic (black solid line) at higher values of η_{PL}. Dashed colored lines in panel 'c' show the calculations for η_{PL} = 90% and Q_{LSC} = 18 (red) and η_{PL} = 70% and Q_{LSC} = 108 (black); these calculations illustrate that the drop in the PL quantum yield can be mitigated by increasing Q_{LSC}, which could allow for increasing the practical device dimensions to the same value as for the ideal emitters with η_{PL} = 100%, but a lower LSC quality factor.

efficiency of 100%. Even when η_{PL} drops to 70%, it is still possible to achieve the same value of L_0 using fluorophores with Q_{LSC} = 108. These considerations highlight an important role, which might be played by "LSC-quality-factor engineering" in efforts on the realization of large area devices utilizing practically available nonideal emitters with η_{PL} less than unity.

The above analysis indicates that the analytical model introduced in the previous section allows for an accurate treatment of planar LSC waveguides not only in qualitative but also quantitative terms. Specifically, as illustrated in Figures 2 and 3, it provides an excellent agreement with the MC simulations for a wide range of LSC parameters including lengths up to more than 1000 cm (corresponds to $G > 500$), PL quantum yields between 50 and 100%, and LSC quality factors up to 1000. In addition to the case of the low optical density waveguide considered in Figures 2 and 3 (optical density 0.1 for incident light), in Figure S2 of SI, we show calculations conducted for a range of optical densities that correspond to $\alpha_1 d$ from 0.01 to 10 using η_{PL} = 0.5−1, and Q_{LCS} = 1−1000. In all of these cases, we again observe a very close agreement of the analytical model with the MC simulations. As illustrated in the next section, this model greatly simplifies the analysis of experimental data and helps quantify optical efficiencies and concentration factors, and elucidate their dependence on LSC parameters.

NONMONOCHROMATIC INCIDENT LIGHT

While the developed model has been applied here to the situation of a monochromatic single-wavelength light source, in principle, it can be easily extended to the case of spectrally broad illumination including solar light. If incident photon flux is characterized by spectral profile $S_{in}(\lambda)$, then the fraction of absorbed photons can be calculated from

$$\eta_{abs} = \frac{(1-R)\int_{E_g}^{\infty} S_{in}(\lambda)[1-e^{-\alpha(\lambda)d}]d\lambda}{\int_{E_g}^{\infty} S_{in}(\lambda)d\lambda} \quad (5)$$

where E_g is the fluorophore band gap. Equation 5 can be reduced to the single-wavelength case $\eta_{abs} = (1-R)(1-e^{-\langle\alpha_1\rangle d})$ if we introduce a spectrally averaged absorption coefficient defined as

$$\langle\alpha_1\rangle = -\frac{1}{d}\ln\left(\frac{\int_{E_g}^{\infty} S_{in}(\lambda)e^{-\alpha(\lambda)d}d\lambda}{\int_{E_g}^{\infty} S_{in}(\lambda)d\lambda}\right) \quad (6)$$

By replacing α_1 in eqs 1−4 with the spectrally averaged value given by eq 6, one can compute optical efficiency and concentration factors (C, C_{sat}, and C_0) for incident radiation with an arbitrary spectral profile.

EXPERIMENTAL STUDIES OF LSC PERFORMANCE AS A FUNCTION OF LSC QUALITY FACTOR

In the experimental part of this work, we investigated two samples of visible-light (yellow and red) emitting II−VI core/shell QDs and a near-infrared emitting sample of $CuInSe_xS_{2-x}$ QDs ($x \approx 1$); see section 2 of SI for details of the syntheses and samples' characterization. QDs were dissolved in toluene and loaded into 4.0 × 1.0 × 0.5 cm^3 optical cells that were studied as "liquid LSCs" with a geometric gain factor G = 4. The samples were excited at λ_1 = 532 nm by an expanded beam of a continuous wave diode laser, which provided a spatially uniform

DOI: 10.1021/acsphotonics.6b00307
ACS Photonics 2016, 3, 1138−1148

illumination across the 4.0 × 1.0 cm^2 surface. The incident power density was 1−10 mW/cm^2, which corresponded to the excitation regime where the average number of electron−hole pairs per QD was much less than unity and hence the effects of nonradiative multicarrier Auger recombination were negligible. The QD emission was collected through the small 1.0 × 0.5 cm^2 window with an 8″ integrating sphere coupled to a spectrometer (see Methods for details of the measurements).

The yellow-emitting sample (labeled #1; λ_2 = 577 nm) represents $Cd_{0.9}Zn_{0.1}Se/ZnSe_{0.3}S_{0.7}$ QDs with a core diameter of 5.2 nm and a shell thickness of 4.3 nm. Its PL quantum yield is 47%. Based on its absorption spectrum and spectral positions of the excitation source and the center of the PL band (Figure 4a), its LSC quality factor is 1.32. To account for the change in α across the emission band we also introduce a spectrally weighted factor $\langle Q_{LSC}\rangle$, which is calculated using the average value of α_2 determined from

$$\langle \alpha_2 \rangle = \frac{\int S_{PL}(\lambda)\alpha(\lambda)d\lambda}{\int S_{PL}(\lambda)d\lambda} \quad (7)$$

where $S_{PL}(\lambda)$ is the spectral profile of PL. Using eq 7, we find that for sample 1, $\langle Q_{LSC}\rangle$ = 1.64. As we show below, the use of the spectrally weighted Q_{LSC}-factor leads to a better agreement with experimental measurements compared to that obtained with Q_{LSC} measured at the PL peak. The red-emitting sample (#2; λ_2 = 635 nm) comprises a 4.6 nm CdSe core overcoated with a 6.1 nm $Cd_{0.3}Zn_{0.7}Se$ shell followed a final 0.8 nm layer of $ZnSe_{0.5}S_{0.5}$. It is characterized by a higher PL efficiency (η_{PL} = 72%) and a higher LSC quality factor than sample 1. At the PL peak wavelength, Q_{LSC} = 7.6 and $\langle Q_{LSC}\rangle$ = 10.9 (Figure 4a).

We would like to caution that, in certain situations (e.g., a very sharp absorption onset occurring within the emission band), the use of spectral averaging (eq 7) may lead to significant errors. Therefore, in general, in the case of a strong variation of α across the PL band, one should use a single-wavelength version of eqs 1−4 for calculating an optical efficiency and concentration factors, and then conduct spectral averaging over the emission profile. We would like to stress, however, that the averaging of α_1 over the spectrum of incident light introduced earlier (eqs 5 and 6) is valid independent of the spectral shape of either LSC absorption or incident radiation.

In our experiments, we monitor the intensity of the collected light as a function of sample optical density at the excitation wavelength (quantified in terms of $\alpha_1 d$) varied by adjusting the concentration of the QDs in the solution (Figure 4b). The incident flux remains constants during these measurements, therefore, the recoded PL intensities represent a relative measure of the LSC optical efficiency. The experiments reveal a nonmonotonic dependence of η_{PL} on $\alpha_1 d$. Initially, the amount of the collected light increases with optical density as a result of increased number of harvested incident photons. However, eventually this trend reverses due to a progressively increasing role of reabsorption of the guided luminescence. The interplay between the two trends produces a maximum in the dependence of η_{opt} on $\alpha_1 d$, which defines the optimal absorptivity of the devices, $(\alpha_1 d)_{opt}$. As expected, sample 2, which has a higher Q_{LSC}, is characterized by a larger value of $(\alpha_1 d)_{opt}$ (~2 vs ~1 for sample 1). Together with a higher PL quantum yield, this leads to a considerable increase (by a factor of 4.4) in the optical efficiency.

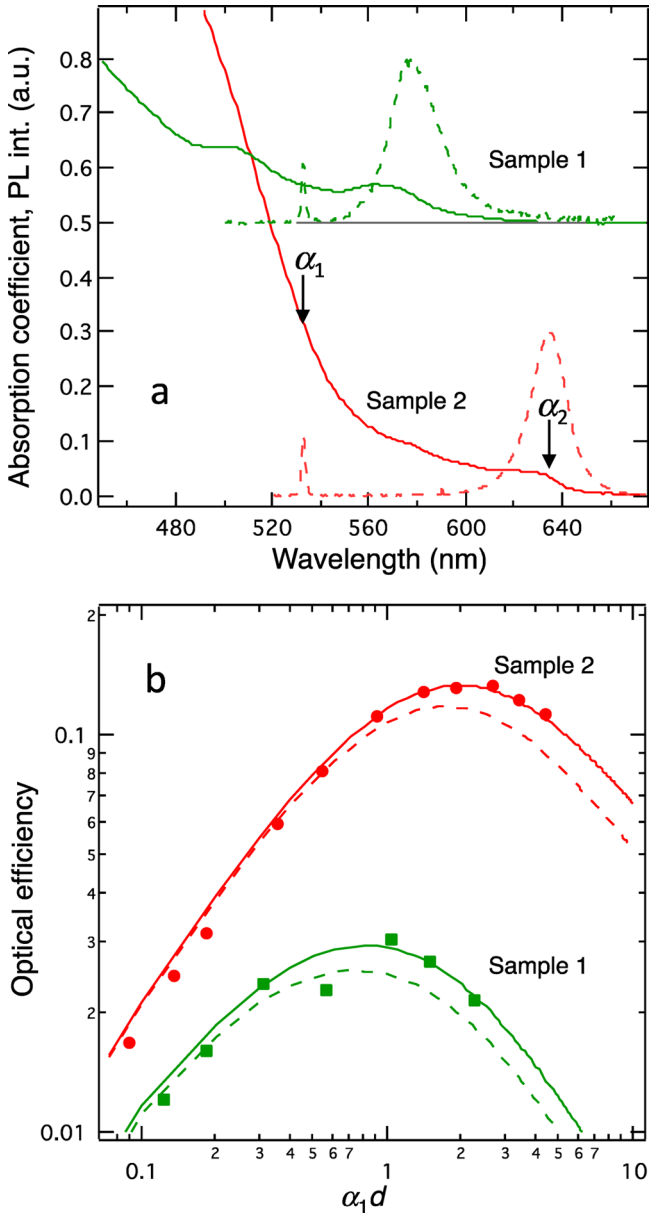

Figure 4. (a) Absorption (solid lines) and PL (dashed lines) spectra of II−VI core−shell QDs characterized by $\langle Q_{LSC}\rangle$ = 1.64 (sample 1, green lines) and 10.9 (sample 2, red lines); see text for detailed sample descriptions. The spike at 532 nm is residual laser emission used to excite the samples. (b) Measured (symbols) and calculated (lines) optical efficiencies of LSCs utilizing samples 1 (green) and 2 (red). Dashed lines correspond to calculations for the LSC quality factors determined based on α_2 at the center of the PL band, while solid lines are for spectrally weighted α_2 (eq 7).

The results of these measurements can be very accurately described using the analytical theory introduced in the previous sections. We would like to remind readers that the original model considers the situation of perfectly reflecting sidewalls, while the studied samples have uncoated glass on all sides. To quantitatively account for this difference, we have conducted MC modeling of LSCs with two types of sidewalls; in one case, they were treated as glass/air interfaces and in the other as perfect mirrors. The results of these calculations are summarized in Figure S3 (fixed L, varied $\alpha_1 d$) and Figure S4 (fixed $\alpha_1 d$, varied L). They indicate that optical efficiencies for the glass/air interface can be perfectly replicated based on

DOI: 10.1021/acsphotonics.6b00307
ACS Photonics 2016, 3, 1138−1148

calculations for the perfect-mirror case if the latter are scaled (divided) by a constant factor 2.53 ± 0.21.

By applying this scaling coefficient to eq 1 and using parameters of our QD samples, we calculate η_{opt} as a function of $\alpha_1 d$. In these calculations, we use β = 1.4, which was found earlier allows for a good agreement with MC simulations for small LSC lengths. First we compute η_{opt} using the Q_{LSC} factors determined based on α_2 at the peak of the PL band (dashed lines in Figure 4b) and then compare them to relative efficiencies determined experimentally after the latter are scaled so as to match the calculations at $\alpha_1 d$ of 0.3−0.4. After implementing this procedure, we observe that the theory describes the experimental data fairly accurately at lower values of $\alpha_1 d$, however, it noticeably deviates from the measurements at higher optical densities. It turns out this discrepancy disappears if we use the spectrally averaged LSC quality factors which allows for a remarkably close agreement with experimental observations (solid lines in Figure 4b). On the basis of this modeling, we can quantify optical efficiencies realized in our experiments. For example, the maximum value of η_{opt} for sample 1 is 3%, while it is improved to 13% in the case of sample 2. We can further project that in the case of fully reflecting side walls the optical efficiencies for these two samples will be increased to 7.5% and 32.5%, respectively. Finally, based on eq 4, the maximum concentration factors achievable with samples 1 and 2 are approximately 0.45 and 6.5 (estimated using β = 1.8).

The improved LSC performance of sample 2 is a result of both the improved PL quantum yield and a higher quality factor. In order to isolate the effects that are solely due to a varied Q_{LSC}, we exploit a large PL bandwidth of the $CuInSe_xS_{2-x}$ QD sample, which allows us to conduct spectrally resolved measurements of the optical efficiency by tuning the detection wavelength within the emission profile (Figure 5a). In the case of the dilute QD solution the PL peak is at 750 nm, and the emission efficiency is 45%. As optical density is progressively increased, the peak shifts to longer wavelengths, which is accompanied by the narrowing of the PL band (Figure S5a of SI). Both observations are indicative of spectrally nonuniform reabsorption, which decreases for longer λ. This can be reinterpreted in terms of the spectrally dependent LSC factor, which increases as the emission wavelength is increased.

To gain a more quantitative insight in the observed PL behavior, we conduct $\alpha_1 d$-dependent measurements of the outcoupled light intensities for wavelengths from 650 to 800 nm, changing λ_2 in 25 nm increments. On the basis of the absorption spectrum (Figure 5a), this corresponds to Q_{LSC} varied from 2.1 to 74.2. The raw unprocessed results of these measurements are displayed in Figure S5b of SI. In order to convert them into relative optical efficiencies, we normalize the data sets acquired for each wavelength by the respective signal amplitudes determined from the PL profile approximated by a Gaussian band (Figure 5a, solid red line; spectral amplitudes used in the normalization are shown by solid circles). The results obtained by this procedure are displayed in Figure 5b (symbols).

Next, we compare these data to calculations based on eq 1 using as before β = 1.4 and including the 0.4 (≈1/2.53) correction factor, which accounts for light losses through the glass side walls, as discussed earlier. We again observe a remarkable agreement between the calculations and the measurements, which allows us to quantify the maximum experimental concentration factors (C_{max}) in absolute terms

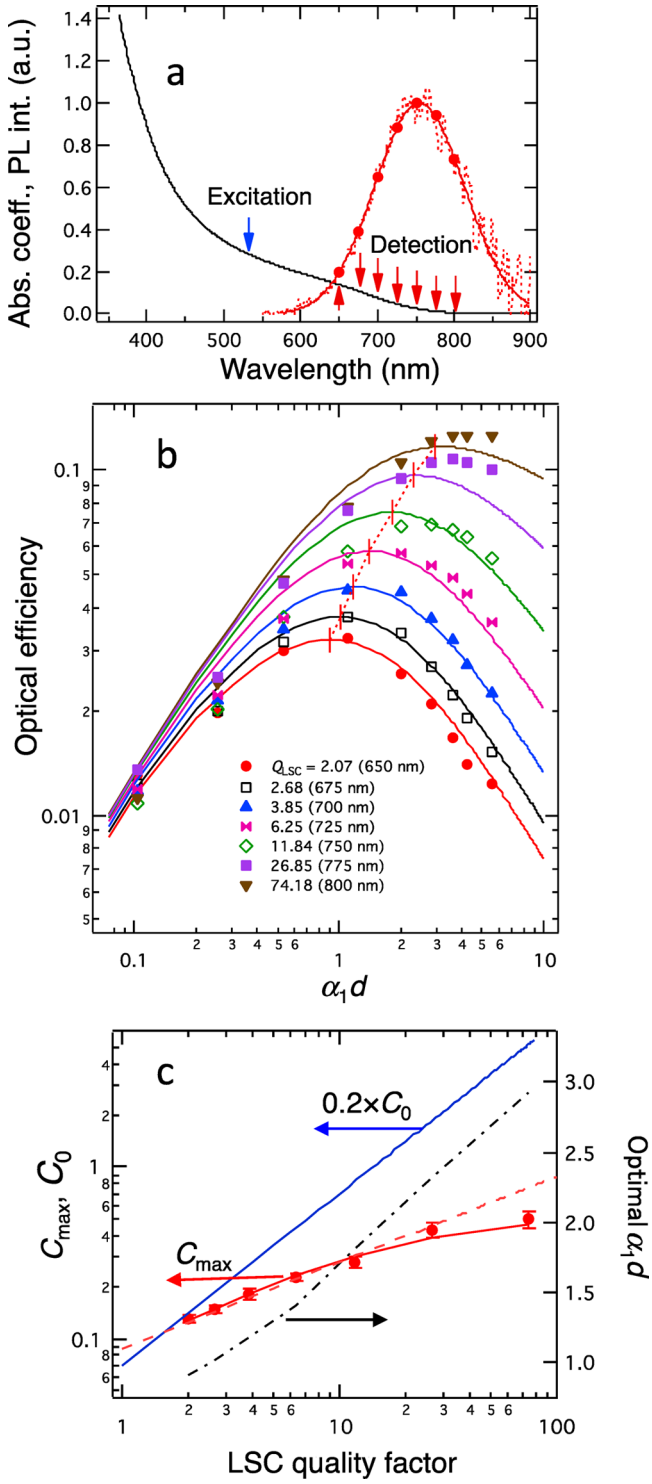

Figure 5. (a) Absorption (black solid line) and PL (red dashed line) spectra of $CuInSe_xS_{2-x}$ QDs ($x \approx 1$); the red solid line is a Gaussian fit of the PL band. The blue arrow marks the spectral position of incident light, while the red arrows mark detection wavelengths used in spectrally resolved measurements of LSC optical efficiencies; circles show the PL amplitudes used to normalize the output signal for quantifying relative values of the optical efficiency (shown in panel "b"). (b) Measured (symbols) and calculated (solid lines) optical efficiencies of the $CuInSe_xS_{2-x}$ QD LCS for a varied detection wavelength (indicated in the figure) as a function of $\alpha_1 d$. The change in the detection wavelengths leads to changes in the LSC quality factor (indicated in the figure), which allows one to isolate the effect of Q_{LSC} on η_{opt} from effects of other parameters such as the PL quantum yield.

DOI: 10.1021/acsphotonics.6b00307
ACS Photonics 2016, 3, 1138−1148

Figure 5. continued

Vertical red bars mark the peak values of optical efficiencies and optimal values of $\alpha_1 d$ for which they are realized. (c) Maximum concentration factor (C_{max}) vs Q_{LSC} as inferred from the measurements (symbols) in comparison to calculations (red solid line); in the range of Q_{LSC} < 20−30, the observed trend can be approximated by the square-root dependence (red dashed line). The black dashed-and-dotted line shows values of $(\alpha_1 d)_{opt}$ that correspond to C_{max}. The blue solid line is an ultimate concentration factor, C_0 (see eq 4), as a function of Q_{LSC}.

and then directly relate them to experimental values of Q_{LSC} varied by changing the detection wavelength (Figure 5c, symbols). We also calculate theoretical values of C_{max} based on eq 2. To do so, we first find an optimal value of optical density, $(\alpha_1 d)_{opt}$, which maximizes C for a given Q_{LSC} (black dashed-and-dotted line in Figure 5c), and then use it to compute C_{max} (red solid line in Figure 5c). The theory once again is in a very close agreement with the experimental findings. Both sets of data show direct scaling of C_{max} with Q_{LSC}. In the range of low and moderate quality factors (Q_{LSC} up to ∼20), this scaling can be approximated by a square-root dependence (red dashed line), while for higher Q_{LSC}, the concentration shows signs of saturation reaching the maximum of ∼0.5 at Q_{LSC} = 74.2. We would like to point out that C_{max} inferred from our measurements of small-size LSCs are different from the ultimate concentration factors (C_0; eq 4) realized in the long-LSC limit when $\alpha_2 L = \alpha_1 d(Q_{LSC})^{-1} \gg 1$. To highlight this difference, we show C_0 derived from eq 4 for the parameters of our $CISe_xS_{1-x}$ QD sample in Figure 5c (blue solid line). As was discussed earlier, C_0 scales linearly with Q_{LSC} and is considerably higher than the values realized in the studied small size LSCs. For example, the ultimate concentration limit for this type of the QDs realized for Q_{LSC} = 74.2 is ∼26.

To summarize, we have used QD-based LSCs to analyze optical efficiencies (η_{opt}) and concentration factors (C) in relation to an LSC quality factor defined as the ratio of absorption coefficients at the wavelengths of incident and emitted light: $Q_{LSC} = \alpha_1/\alpha_2$. In this analysis, we utilize an analytical model, which allows us to quantify LSC performance (e.g., in terms of η_{opt} and C) based on Q_{LSC}, PL quantum yield, geometric gain factor, and the device absorptivity at the wavelength of the incident light. We find that, in all of the considered cases, this theory is in excellent agreement with numerical MC ray-tracing simulations. However, as compared to the computationally intense MC modeling, the analytical allows for a much faster evaluation of prospective performance of LSCs based on the optical spectra of light emitting fluorophores and geometrical parameters of the LSC slabs. This greatly simplifies analysis of experimental data and can, in principle, help in the optimization of both the optical properties of LCS fluorophores and the waveguide design in practical devices.

The analysis of both theoretical and experimental data indicates that the concentration factor scales directly with the LSC quality factor. Specifically, we show that the ultimate concentration limit (C_0) realized in large-size LSCs ($\alpha_2 L \gg 1$) is directly proportional to Q_{LSC}, and in the case of perfect emitters (η_{PL} = 100%) and the simplest LSC design, which does not employ selective reflectors on the top of the structure or fully reflecting mirrors on its back side, $C_0 \approx Q_{LSC}$. We also consider the case of a fixed LSC size and a given Q_{LSC}, where the LSC performance can be optimized to maximize η_{opt} and C by adjusting the absorption coefficient for incident light. We find that C_{max} realized in this case also scales directly with Q_{LSC}, however, slower than in the C_0 case. Specifically, both measurements and calculations indicate that in the range of small and moderately high Q_{LSC}-factor (Q_{LSC} < 20−30), the dependence of C on Q_{LSC} can be approximated by a square-root function. The results of this work provide quantitative guidelines for predicting LSC efficiencies based on optical properties of LSC fluorophores and the geometry of the LSC waveguides. This should aid in the development of practical devices for applications as both semitransparent PV windows and nearly opaque high-concentration systems.

METHODS

Optical Characterization. Different concentrations of QDs were prepared in toluene and loaded into 4.0 × 1.0 × 0.5 cm^3 quartz fluorimeter cuvettes (Starna, 23-Q-5). Toluene was chosen over other solvents to more closely match the index of the quartz cuvette and thus minimize any effects due to refractive index mismatch. Absorption spectra of the samples were taken on a diode array UV−vis spectrometer. Emission from QD samples was excited with a continuous-wave 532 nm diode laser (LaserGlow). The pump beam was expanded to the 1″ size by a Newtonian telescope and then transmitted through a 2″ aspheric condenser with a diffuser (Thorlabs, ACL504OU-DG6) to produce a large area collimated light source to uniformly illuminate the 4.0 × 1.0 cm^2 side of the cuvette. The spatial uniformity of the illumination was verified by translating a 1 cm diameter power meter in the sample plane. The power was found to fluctuate by less than 5% across the sample excitation area. The incident power was attenuated with neutral density filters to 1−10 mW/cm^2 at the sample surface.

The cuvette with QDs was held vertically by a specially designed holder that allowed for direct mounting onto the integrating sphere entrance port while minimally obscuring the excitation area. In this manner, light incident on the largest area surface of the cuvette was absorbed by the QDs and the fluorescence escaping the bottom surface was directed into one port of an 8″ integrating sphere (Labsphere). The PL intensity was measured using a second port, which was equipped with a fiber optic coupler connected to a spectrometer (Ocean Optics, JAZZ). The spectral sensitivity of the joint instrument (spectrometer, fiber, and integrating sphere) was calibrated using the output of a standard light source (certified, white light Tungsten bulb).

ASSOCIATED CONTENT

Supporting Information

The Supporting Information is available free of charge on the ACS Publications website at DOI: 10.1021/acsphotonics.6b00307.

QD sample fabrication procedures, characterization of the QD samples using transmission electron microscopy, analytical and Monte Carlo modeling of optical efficiencies of luminescent solar concentrators as a function of device length and optical density for varied photoluminescence quantum yields, derivation of correction factors for relating optical efficiencies of devices with perfectly reflecting sidewalls to those with uncoated glass sidewalls, and the measurements of a

DOI: 10.1021/acsphotonics.6b00307
ACS Photonics 2016, 3, 1138−1148

spectrally resolved PL intensity as a function of optical density of the $CuInSe_xS_{2-x}$QD sample (PDF).

AUTHOR INFORMATION

Corresponding Author

*E-mail: klimov@lanl.gov.

Notes

The authors declare no competing financial interest.

ACKNOWLEDGMENTS

This work was supported by the Center for Advanced Solar Photophysics (CASP), an Energy Frontier Research Center funded by the U.S. Department of Energy, Office of Science, Basic Energy Sciences.

REFERENCES

(1) Weber, W.; Lambe, J. Luminescent Greenhouse Collector for Solar Radiation. *Appl. Opt.* **1976**, *15*, 2299−2300.

(2) Hermann, A. M. Luminescent Solar Concentrators - a Review. *Sol. Energy* **1982**, *29*, 323−329.

(3) Batchelder, J. S.; Zewail, A. H.; Cole, T. Luminescent Solar Concentrators 0.2. Experimental and Theoretical-Analysis of Their Possible Efficiencies. *Appl. Opt.* **1981**, *20*, 3733−3754.

(4) Batchelder, J. S.; Zewai, A. H.; Cole, T. Luminescent Solar Concentrators 0.1. Theory of Operation and Techniques for Performance Evaluation. *Appl. Opt.* **1979**, *18*, 3090−3110.

(5) van Sark, W. G. J. H. M.; Barnham, K. W. J.; Slooff, L. H.; Chatten, A. J.; Buchtemann, A.; Meyer, A.; McCormack, S. J.; Koole, R.; Farrell, D. J.; Bose, R.; Bende, E. E.; Burgers, A. R.; Budel, T.; Quilitz, J.; Kennedy, M.; Meyer, T.; Donega, C. D. M.; Meijerink, A.; Vanmaekelbergh, D. Luminescent Solar Concentrators - a Review of Recent Results. *Opt. Express* **2008**, *16*, 21773−21792.

(6) Debije, M. G.; Verbunt, P. P. C. Thirty Years of Luminescent Solar Concentrator Research: Solar Energy for the Built Environment. *Adv. Energy Mater.* **2012**, *2*, 12−35.

(7) Rau, U.; Einsele, F.; Glaeser, G. C. Efficiency Limits of Photovoltaic Fluorescent Collectors. *Appl. Phys. Lett.* **2005**, *87*, 171101.

(8) Markvart, T. Detailed Balance Method for Ideal Single-Stage Fluorescent Collectors. *J. Appl. Phys.* **2006**, *99*, 026101.

(9) Shockley, W.; Queisser, H. J. Detailed Balance Limit of Efficiency of p-n Junction Solar Cells. *J. Appl. Phys.* **1961**, *32*, 510−519.

(10) Chemisana, D. Building Integrated Concentrating Photovoltaics: A Review. *Renewable Sustainable Energy Rev.* **2011**, *15*, 603−611.

(11) Meinardi, F.; McDaniel, H.; Carulli, F.; Colombo, A.; Velizhanin, K. A.; Makarov, N. S.; Simonutti, R.; Klimov, V. I.; Brovelli, S. Highly Efficient Large-Area Colourless Luminescent Solar Concentrators Using Heavy-Metal-Free Colloidal Quantum Dots. *Nat. Nanotechnol.* **2015**, *10*, 878−885.

(12) Leow, S. W.; Corrado, C.; Osborn, M.; Carter, S. A. Monte Carlo Ray-Tracing Simulations of Luminescent Solar Concentrators for Building Integrated Photovoltaics. *Proc. SPIE* **2013**, *8821*, 882103−882107.

(13) Bomm, J.; Büchtemann, A.; Chatten, A. J.; Bose, R.; Farrell, D. J.; Chan, N. L. A.; Xiao, Y.; Slooff, L. H.; Meyer, T.; Meyer, A.; van Sark, W. G. J. H. M.; Koole, R. Fabrication and Full Characterization of State-of-the-Art Quantum Dot Luminescent Solar Concentrators. *Sol. Energy Mater. Sol. Cells* **2011**, *95*, 2087−2094.

(14) Currie, M. J.; Mapel, J. K.; Heidel, T. D.; Goffri, S.; Baldo, M. A. High-Efficiency Organic Solar Concentrators for Photovoltaics. *Science* **2008**, *321*, 226−228.

(15) Gallagher, S. J.; Rowan, B. C.; Doran, J.; Norton, B. Quantum Dot Solar Concentrator: Device Optimisation Using Spectroscopic Techniques. *Sol. Energy* **2007**, *81*, 540−547.

(16) Krumer, Z.; Pera, S. J.; van Dijk-Moes, R. J. A.; Zhao, Y. M.; de Brouwer, A. F. P.; Groeneveld, E.; van Sark, W. G. J. H. M.; Schropp, R. E. I.; Donega, C. D. Tackling Self-Absorption in Luminescent Solar Concentrators with Type-II Colloidal Quantum Dots. *Sol. Energy Mater. Sol. Cells* **2013**, *111*, 57−65.

(17) Erickson, C. S.; Bradshaw, L. R.; McDowall, S.; Gilbertson, J. D.; Gamelin, D. R.; Patrick, D. L. Zero-Reabsorption Doped-Nanocrystal Luminescent Solar Concentrators. *ACS Nano* **2014**, *8*, 3461−3467.

(18) Bronstein, N. D.; Yao, Y.; Xu, L.; O'Brien, E.; Powers, A. S.; Ferry, V. E.; Alivisatos, A. P.; Nuzzo, R. G. Quantum Dot Luminescent Concentrator Cavity Exhibiting 30-Fold Concentration. *ACS Photonics* **2015**, *2*, 1576−1583.

(19) Bronstein, N. D.; Li, L.; Xu, L.; Yao, Y.; Ferry, V. E.; Alivisatos, A. P.; Nuzzo, R. G. Luminescent Solar Concentration with Semiconductor Nanorods and Transfer-Printed Micro-Silicon Solar Cells. *ACS Nano* **2014**, *8*, 44−53.

(20) Sahin, D.; Ilan, B.; Kelley, D. F. Monte-Carlo Simulations of Light Propagation in Luminescent Solar Concentrators Based on Semiconductor Nanoparticles. *J. Appl. Phys.* **2011**, *110*, 033108.

(21) Meinardi, F.; Colombo, A.; Velizhanin, K. A.; Simonutti, R.; Lorenzon, M.; Beverina, L.; Viswanatha, R.; Klimov, V. I.; Brovelli, S. Large-Area Luminescent Solar Concentrators Based on 'Stokes-Shift-Engineered' Nanocrystals in a Mass-Polymerized PMMA Matrix. *Nat. Photonics* **2014**, *8*, 392−399.

(22) Coropceanu, I.; Bawendi, M. G. Core/Shell Quantum Dot Based Luminescent Solar Concentrators with Reduced Reabsorption and Enhanced Efficiency. *Nano Lett.* **2014**, *14*, 4097−4101.

(23) Bradshaw, L. R.; Knowles, K. E.; McDowall, S.; Gamelin, D. R. Nanocrystals for Luminescent Solar Concentrators. *Nano Lett.* **2015**, *15*, 1315−1323.

(24) Wang, C. H.; Shcherbatyuk, G.; Inman, R.; Pelka, D.; Zhang, W. Y.; Rodriguez, Y.; Carter, S.; Winston, R.; Ghosh, S. Efficiency Improvement by Near Infrared Quantum Dots for Luminescent Solar Concentrators. *Proc. SPIE* **2010**, *7772*, 77720G−77726G.

(25) Sholin, V.; Olson, J. D.; Carter, S. A. Semiconducting Polymers and Quantum Dots in Luminescent Solar Concentrators for Solar Energy Harvesting. *J. Appl. Phys.* **2007**, *101*, 123114.

(26) Aldakov, D.; Lefrancois, A.; Reiss, P. Ternary and Quaternary Metal Chalcogenide Nanocrystals: Synthesis, Properties and Applications. *J. Mater. Chem. C* **2013**, *1*, 3756−3776.

(27) Yarema, O.; Bozyigit, D.; Rousseau, I.; Nowack, L.; Yarema, M.; Heiss, W.; Wood, V. Highly Luminescent, Size- and Shape-Tunable Copper Indium Selenide Based Colloidal Nanocrystals. *Chem. Mater.* **2013**, *25*, 3753−3757.

(28) Li, L.; Daou, T. J.; Texier, I.; Tran, T. K. C.; Nguyen, Q. L.; Reiss, P. Highly Luminescent $CuInS_2$/Zns Core/Shell Nanocrystals: Cadmium-Free Quantum Dots for in Vivo Imaging. *Chem. Mater.* **2009**, *21*, 2422−2429.

(29) Pietryga, J. M.; Werder, D. J.; Williams, D. J.; Casson, J. L.; Schaller, R. D.; Klimov, V. I.; Hollingsworth, J. A. Utilizing the Lability of Lead Selenide to Produce Heterostructured Nanocrystals with Bright, Stable Infrared Emission. *J. Am. Chem. Soc.* **2008**, *130*, 4879−4885.

(30) Semonin, O. E.; Johnson, J. C.; Luther, J. M.; Midgett, A. G.; Nozik, A. J.; Beard, M. C. Absolute Photoluminescence Quantum Yields of IR-26 Dye, PbS, and PbSe Quantum Dots. *J. Phys. Chem. Lett.* **2010**, *1*, 2445−2450.

(31) Li, L. A.; Pandey, A.; Werder, D. J.; Khanal, B. P.; Pietryga, J. M.; Klimov, V. I. Efficient Synthesis of Highly Luminescent Copper Indium Sulfide-Based Core/Shell Nanocrystals with Surprisingly Long-Lived Emission. *J. Am. Chem. Soc.* **2011**, *133*, 1176−1179.

(32) Li, C.; Chen, W.; Wu, D.; Quan, D. H.; Zhou, Z. M.; Hao, J. J.; Qin, J.; Li, Y. W.; He, Z. B.; Wang, K. Large Stokes Shift and High Efficiency Luminescent Solar Concentrator Incorporated with $CuInS_2$/ZnS Quantum Dots. *Sci. Rep.* **2015**, *5*, 17777.

(33) Rice, W. D.; McDaniel, H.; Klimov, V. I.; Crooker, S. A. Magneto-Optical Properties of $CuInS_2$ Nanocrystals. *J. Phys. Chem. Lett.* **2014**, *5*, 4105−4109.

(34) Yablonovitch, E. Thermodynamics of the Fluorescent Planar Concentrator. *J. Opt. Soc. Am.* **1980**, *70*, 1362−1363.

DOI: 10.1021/acsphotonics.6b00307
ACS Photonics 2016, 3, 1138−1148

(35) Smestad, G.; Ries, H.; Winston, R.; Yablonovitch, E. The Thermodynamic Limits of Light Concentrators. *Sol. Energy Mater.* **1990**, *21*, 99−111.
(36) Ries, H. Thermodynamic Limitations of the Concentration of Electromagnetic-Radiation. *J. Opt. Soc. Am.* **1982**, *72*, 380−385.
(37) Chatten, A. J.; Barnham, K. W. J.; Buxton, B. F.; Ekins-Daukes, N. J.; Malik, M. A. A New Approach to Modelling Quantum Dot Concentrators. *Sol. Energy Mater. Sol. Cells* **2003**, *75*, 363−371.
(38) Barnham, K.; Marques, J. L.; Hassard, J.; O'Brien, P. Quantum-Dot Concentrator and Thermodynamic Model for the Global Redshift. *Appl. Phys. Lett.* **2000**, *76*, 1197−1199.
(39) Scudo, P. F.; Abbondanza, L.; Fusco, R.; Caccianotti, L. Spectral Converters and Luminescent Solar Concentrators. *Sol. Energy Mater. Sol. Cells* **2010**, *94*, 1241−1246.
(40) Xu, L.; Yao, Y.; Bronstein, N. D.; Li, L. F.; Alivisatos, A. P.; Nuzzo, R. G. Enhanced Photon Collection in Luminescent Solar Concentrators with Distributed Bragg Reflectors. *ACS Photonics* **2016**, *3*, 278−285.
(41) Sansregret, J.; Drake, J. M.; Thomas, W. R. L.; Lesiecki, M. L. Light Transport in Planar Luminescent Solar Concentrators - the Role of DCM Self-Absorption. *Appl. Opt.* **1983**, *22*, 573−577.
(42) Carrascosa, M.; Unamuno, S.; Agullolopez, F. Monte-Carlo Simulation of the Performance of Pmma Luminescent Solar Collectors. *Appl. Opt.* **1983**, *22*, 3236−3241.
(43) Smestad, G.; Hamill, P. Concentration of Solar-Radiation by White Backed Photovoltaic Panels. *Appl. Opt.* **1984**, *23*, 4394−4402.
(44) Smestad, G.; Hamill, P. Concentration of Solar-Radiation by White Painted Transparent Plates. *Appl. Opt.* **1982**, *21*, 1298−1306.

DOI: 10.1021/acsphotonics.6b00307
ACS Photonics 2016, 3, 1138−1148